ACS APPLIED MATERIALS & INTERFACES

Research Article

Cite This: ACS Appl. Mater. Interfaces 2018, 10, 37555−37565

www.acsami.org

Thermal Percolation Threshold and Thermal Properties of Composites with High Loading of Graphene and Boron Nitride Fillers

Fariborz Kargar,[†,‡,∥] Zahra Barani,[†,‡,∥] Ruben Salgado,[†,‡] Bishwajit Debnath,[§] Jacob S. Lewis,[†,‡] Ece Aytan,[†,‡] Roger K. Lake,[§] and Alexander A. Balandin*[,†,‡]

[†]Phonon Optimized Engineered Materials (POEM) Center, Materials Science and Engineering Program, University of California, Riverside, California 92521, United States

[‡]Nano-Device Laboratory (NDL), Department of Electrical and Computer Engineering, University of California, Riverside, California 92521, United States

[§]Laboratory for Terascale and Terahertz Electronics (LATTE), Department of Electrical and Computer Engineering, University of California, Riverside, California 92521, United States

Supporting Information

ABSTRACT: We investigated thermal properties of the epoxy-based composites with the high loading fraction—up to $f \approx 45$ vol %—of the randomly oriented electrically conductive graphene fillers and electrically insulating boron nitride fillers. It was found that both types of the composites revealed a distinctive *thermal* percolation threshold at the loading fraction $f_T > 20$ vol %. The graphene loading required for achieving thermal percolation, f_T, was substantially higher than the loading, f_E, for *electrical* percolation. Graphene fillers outperformed boron nitride fillers in the thermal conductivity enhancement. It was established that thermal transport in composites with high filler loadings, $f \geq f_T$, is dominated by heat conduction via the network of percolating fillers. Unexpectedly, we determined that the thermal transport properties of the high loading composites were influenced strongly by the cross-plane thermal conductivity of the quasi-two-dimensional fillers. The obtained results shed light on the debated mechanism of the thermal percolation, and facilitate the development of the next generation of the efficient thermal interface materials for electronic applications.

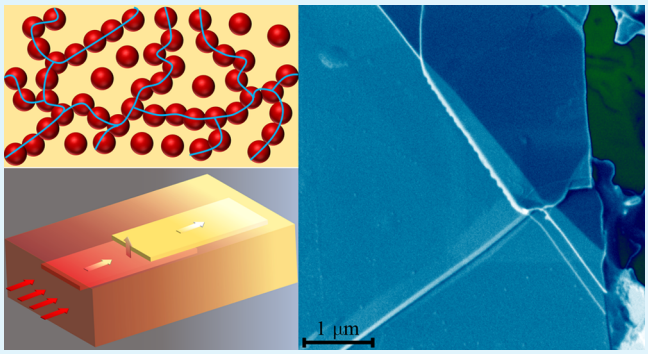

KEYWORDS: *thermal conductivity, thermal percolation, graphene, boron nitride, thermal diffusivity, thermal management*

INTRODUCTION

The discovery of unique heat conduction properties of graphene[1−7] motivated numerous practically oriented studies of the use of graphene and few-layer graphene (FLG) in various composites, thermal interface materials, and coatings.[8−15] The intrinsic thermal conductivity of large graphene layers exceeds that of the high-quality bulk graphite, which by itself is very high: 2000 W m^{-1} K^{-1} at room temperature (RT).[1,11,16,17] The first studies of graphene composites found that even small loading fractions of randomly oriented graphene fillers—up to $f = 10$ vol %—can increase the thermal conductivity of epoxy composites by up to a factor of ×25 [ref 11]. These results have been independently confirmed by different research groups.[18,19] The variations in the reported thermal data for graphene composites can be explained by the differences in the methods of preparation, matrix materials, quality of graphene, lateral sizes and thickness of graphene fillers, and other factors.[3,20−25] Most of the studies of thermal composites with graphene have been limited to the relatively low loading fractions, $f \leq 10$ vol %. The latter was due to difficulties in preparation of high-loading fraction composites with a uniform dispersion of graphene flakes. The changes in viscosity and graphene flake agglomeration complicated the synthesis of a consistent set of samples with the loading substantially above $f = 10$ vol %.

Investigation of thermal properties of composites with the high loading fraction of graphene or FLG fillers is interesting from both fundamental science and practical applications points of view. A high filler loading is required for understanding the thermal percolation in composites with graphene and other two-dimensional (2D) materials. Thermal percolation in composites, in general, remains a rather

Received: September 23, 2018
Accepted: October 9, 2018
Published: October 9, 2018

DOI: 10.1021/acsami.8b16616
ACS Appl. Mater. Interfaces 2018, 10, 37555−37565

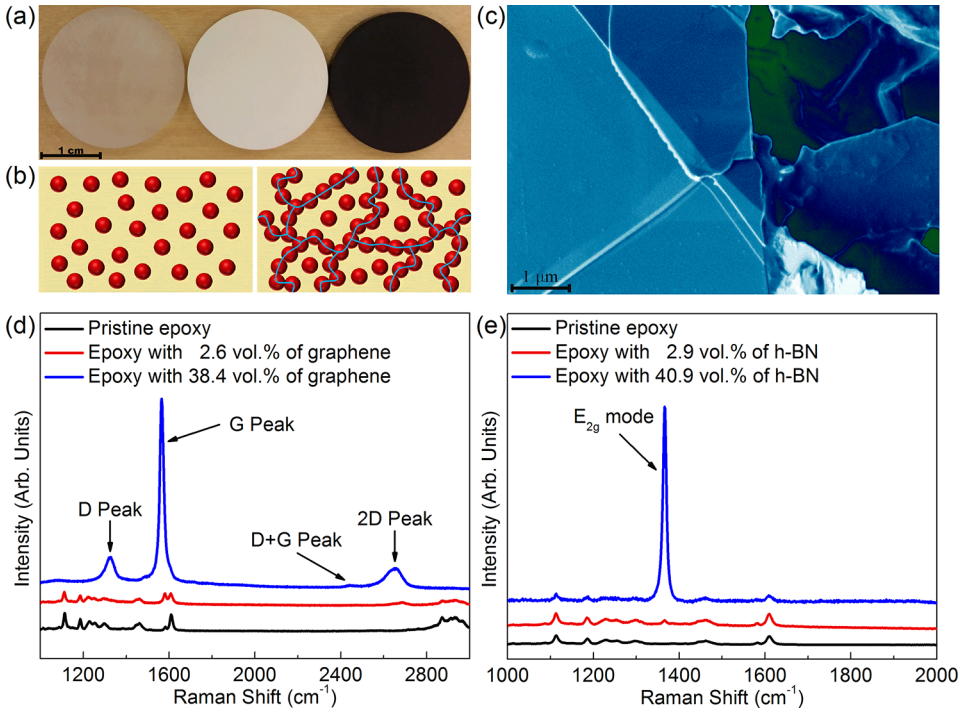

Figure 1. (a) Optical image of the pristine epoxy, and epoxy with the loading of 18 vol % and 19 vol % of graphene and *h*-BN fillers, respectively. Note a distinctively black color of graphene composite as opposed to the white color of *h*-BN composite. (b) Schematic of the composite with the low (left) and high (right) volume fraction of fillers. (c) Scanning electron microscopy image of the epoxy composite with 45 vol % of graphene fillers. The microscopy image of the high-loading composites shows clearly the overlapping of graphene fillers inside the epoxy matrix. The overlapping fillers confirm the formation of the percolation network at this high loading fraction of graphene. Raman spectra of (d) pristine epoxy and epoxy with the low and high graphene filler loading fraction; and (e) pristine epoxy and epoxy with the low and high *h*-BN filler loading fraction. The peak at 1366 cm^{-1} is the E_{2g} vibration mode of *h*-BN. In both types of composites, the higher loading of fillers resulted in the increased intensity of the characteristic graphene or *h*-BN phonon peaks allowing for additional verification of the composition of the samples.

controversial issue.[26−34] The electrical percolation in composites with various carbon fillers, including carbon nanotubes and graphene, can be clearly observed experimentally as an abrupt change in the electrical conductivity.[35−41] It is commonly described theoretically by the power scaling law[35−41] $\sigma \sim (f - f_E)^t$, where σ is the electrical conductivity of the composite, f is the filler loading volume fraction, f_E is the filler loading fraction at the electrical percolation threshold, and t is the "universal" critical exponent in which $t \approx 2$ represents the percolation in three dimensions.[35,37] However, in most of cases, the thermal conductivity of composites does not reveal such obvious changes as the loading fraction continues to increase. There have been suggestions that thermal percolation threshold does not exist at all.[27] The common argument is that the electrically insulating matrix materials do not conduct electrical current but still conduct heat. Indeed, the ratio of the intrinsic thermal conductivity of graphene fillers, K_f, to that of the epoxy matrix, K_m, is $K_f/K_m \sim 10^5$. The ratio of the electrical conductivity of the graphene fillers to that of the matrix can be as high as $\sigma_f/\sigma_m \sim 10^{15}$. With such a difference in the ratios, the electrical conduction is only expected via the percolation network while the thermal conduction can still happen through the matrix.[27,42] Even if thermal percolation is achieved, it is still an open question of how much of the heat flux is propagating via the percolated network of fillers in comparison with the thermal transport though the matrix.

There is also a very strong practical motivation for research of composites with a high loading of graphene. There is an ever-increasing demand for better thermal interface materials (TIMs) for heat removal in electronics and energy conversion applications.[2,10,43,44] Commercially available TIMs with the "bulk" thermal conductivity in the range from ∼0.5 W m^{-1} K^{-1} to 5 W m^{-1} K^{-1} no longer meet the industry requirements. Composites with a high loading of graphene fillers have the potential to deliver high thermal conductivity and low thermal contact resistance. Moreover, recent technological developments have demonstrated that liquid phase exfoliated (LPE) graphene can be produced inexpensively and in large quantities.[45,46] Various methods of reduction of graphene oxide (GO) have also been reported.[41,47−49] The progress in graphene and GO synthesis made FLG fillers practical even for the composites with high loading fractions. One should note here that FLG fillers with a thickness in the range of a few nanometers are substantially different from milled graphite fillers with hundreds of nanometers or micrometer thicknesses. Much thicker graphite fillers do not have the flexibility of FLG and, as a result, do not couple well to the matrix.

In this article, we report the results of our investigation of heat transport in the epoxy composites with a high loading fraction—up to f = 45 vol %—of graphene and hexagonal boron nitride (*h*-BN) fillers. The second type of fillers—electrically insulating *h*-BN—was used for comparison with the electrically conducting graphene in order to establish the most *general* trends in thermal conductivity of composites with quasi-2D fillers. We established that both types of the composites revealed a distinctive *thermal* percolation threshold at the loading fraction $f_T \approx 30$ vol % for graphene and $f_T \approx 23$ vol % for *h*-BN. The onset of the thermal percolation was achieved at higher loading than the electrical percolation in

DOI: 10.1021/acsami.8b16616
ACS Appl. Mater. Interfaces 2018, 10, 37555−37565

graphene composites. It was found that the thermal conductivity of both composites in the entire range of loading fractions can be best described by the Lewis–Nielsen model.[50,51] We discovered that, contrary to conventional belief, the thermal transport in composites with the filler loading $f \geq f_T$ is influenced strongly by the apparent *cross-plane* thermal conductivity of the quasi-2D fillers such as graphene or boron nitride. At low loading, $f \leq f_T$, most of the fillers are not attached to each other, and the thermal transport is governed by the thermal conductivity of the base polymer and the in-plane thermal conductivity of the fillers.

EXPERIMENTAL SECTION

Materials. In order to achieve the high loading fraction of fillers, we used commercially produced graphene and *h*-BN fillers. In the thermal context, the term "graphene fillers" implies a mixture of graphene and FLG flakes with the lateral size and thicknesses in a certain range, differentiating such fillers from much thicker graphite flakes or nanoplatelet graphite powder. The same terminology convention applies to *h*-BN fillers. The composite samples were prepared from the commercially produced graphene flakes (Graphene Supermarket) and *h*-BN flakes (US Research Nanomaterials, Inc.). The lateral size of the few-atomic-layer fillers of graphene ranged from ~2 μm to ~8 μm while the thickness varied from single atomic planes of 0.35 nm to ~12 nm. The lateral dimensions of *h*-BN were comparable, in the interval from ~3 μm to ~8 μm. To obtain a uniform dispersion and avoid air gaps in the high loading composites, we used an in-house designed mixer. The graphene and *h*-BN mixtures were not optimized for achieving the largest thermal conductivity enhancement.[10,11] However, the consistent composition used for samples with all loading fractions allowed us to reveal the percolation trends in such composites.

Composite Characterization. The composites were prepared in the form of disks with a radius of 25.6 mm and thickness of 3 mm (see Figure 1a). We paid particular attention to accurate determination of the mass density of the resulting samples (Figures S1 and S2). The procedures of the sample preparation and characterization are described in detail in the Methods section and Supporting Information. Below the percolation threshold ($f < f_T$), the fillers do not attach to each other, whereas, above it ($f > f_T$), they create a network of pathways for conducting heat (see the schematics in Figure 1b). The samples with different loading fraction of the fillers, *f*, were characterized by the scanning electron microscopy (SEM). Figure 1c shows an SEM image of the sample with a high graphene loading ($f \sim 45$ vol %). One can clearly see the overlapping segments of graphene fillers, indicative of the formation of the percolation network. The composition and quality of the graphene and *h*-BN epoxy composites have been verified with Raman spectroscopy (Renishaw InVia). The representative spectra are shown in Figure 1d,e. The measurements were performed in the backscattering configuration under visible red laser (λ = 633 nm). The excitation power on the surface was kept at ~3.6 mW in all the experiments. In both types of composites, the higher loading of fillers resulted in the increased intensity of the characteristic graphene (G-peak at ~1580 cm^{-1}) or *h*-BN (E_{2g} mode at ~1366 cm^{-1}) phonon peaks, allowing for additional verification of the composition of the samples. It should be noted that, in the case of epoxy with graphene fillers, the intensity of the 2D peak is much lower than the intensity of the G-peak, indicating the random mixture of single- and few-layer graphene flakes inside the epoxy matrix.

RESULTS AND DISCUSSION

Conductivity and Thermal Percolation. The thermal conductivity, *K*, at room temperature (RT) was measured using the transient "hot disk" method.[13,52,53] Details of the measurements are provided in the Methods section and Figure S3. Figure 2a,b shows the thermal conductivity as a function of the filler loading fraction, *f*, for composites with graphene and *h*-BN, respectively. One can see that the thermal conductivity enhancement is stronger in composites with graphene than that with *h*-BN. The maximum thermal conductivity enhancements of ×51 and ×24 are achieved for the epoxy composites with graphene (f = 43 vol %) and *h*-BN (f = 45 vol %), respectively (Figure S4 and Table S1). Better performance of graphene as the filler material can be explained by its higher intrinsic thermal conductivity, which substantially exceeds that of *h*-BN.[1,3,4,54−63] The intrinsic thermal conductivity of large graphene layers was reported to be in the range from 2000 W m^{-1} K^{-1} to 5000 W m^{-1} K^{-1} near RT.[1,3,6] The experimental values reported for thermal conductivity of few-layer *h*-BN were found to vary from ~230 W m^{-1} K^{-1} to ~480 W m^{-1} K^{-1} at RT.[54−57] Theoretical calculations report the thermal conductivity of single-layer to few-layer *h*-BN in the range from ~400 W m^{-1} K^{-1} to ~1000 W m^{-1} K^{-1} [refs 58−63]. The overall functional dependence of the thermal conductivity of the composites on the loading fraction is the same for both fillers—electrically conducting graphene and electrically insulating *h*-BN. This fact can be explained by the negligible

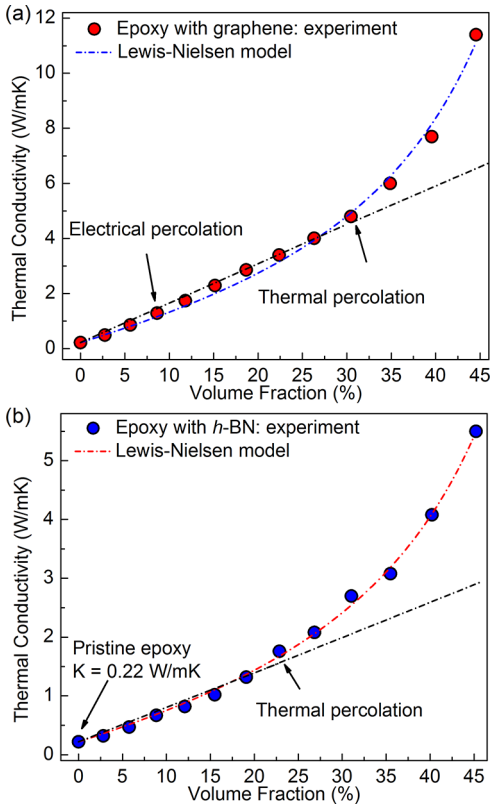

Figure 2. Thermal conductivity of the epoxy composites with (a) graphene and (b) *h*-BN fillers over a wide range of filler loading fraction. The thermal conductivity depends approximately linear on the loading fraction until $f_T \approx 30$ vol % in graphene composites and $f_T \approx 23$ vol % in *h*-BN composites. Above these loading fractions, the dependence becomes super-linear, indicating the onset of the *thermal* percolation transport regime. The maximum thermal conductivity enhancements of ×51 and ×24 are achieved for the epoxy composites with graphene (f = 43 vol %) and *h*-BN (f = 45 vol %), respectively. The blue and red dashed-dotted curves corresponds to the Lewis-Nielsen model. The black dashed-dotted line shows the deviation of the experimental data from initial linear trend of composite thermal conductivity as a function of filler loading fraction.

DOI: 10.1021/acsami.8b16616
ACS Appl. Mater. Interfaces 2018, 10, 37555−37565

contribution of electrons to heat conduction of graphene near RT[2].

The thermal conductivity depends approximately linearly on the loading fraction for $f_T \lesssim 30$ vol % in graphene composites and $f_T \lesssim 23$ vol % in *h*-BN composites. Above these loading fractions, the dependence becomes super-linear (Figures S5 and S6), indicating the onset of the thermal percolation transport regime.[26,28−31,64−67] The change in the thermal conductivity trend is well resolved for both types of the fillers. The functional dependence $K(f)$ is very different from that in a graphite suspension[29] and in the one available prior report of the thermal percolation in graphene.[30] We did not observe singularities in $K(f)$ or $\delta K(f)/\delta f$ dependences but rather an onset of deviation from the linear trend. The measured electrical resistivity in the same composites with graphene revealed the electrical percolation threshold at $f_E \approx 10$ vol %—substantially lower loading than $f_T \approx 30$ vol % (Figure 2a). Another important observation is that, despite the large difference in the intrinsic thermal conductivities of graphene, K_G, and that of *h*-BN, $K_{h\text{-BN}}$ (the ratio $K_G/K_{h\text{-BN}} \geq 5$), the thermal percolation is achieved at approximately the same loading fraction. We explain it by the similar lateral dimensions, thicknesses, geometry, and flexibility of the graphene and *h*-BN fillers. Below, we discuss the results in more detail within the framework of the Lewis−Nielsen model.[50,51]

The obtained thermal conductivity of the epoxy composite with randomly oriented graphene fillers, $K \approx 11$ W m^{-1} K^{-1} at $f = 45$ vol % is rather impressive, and exceeds that of the commercially available TIMs with a similar matrix. This value was obtained with commercial graphene, without additional processing steps. The thermal conductivity of the composites can be further increased at a fixed loading via optimization of the filler lateral sizes and thicknesses.[11] The fillers with lateral sizes exceeding the phonon mean free path (MFP) in a given material are more efficient in heat conduction (see Figure S7 and Table S2). The average "grey" phonon MFP in graphene is ∼800 nm near RT [ref 2]. The latter indicates that the lateral dimensions of the graphene fillers should be larger than ∼1 μm. However, if the lateral dimensions become too large, the fillers can start folding and rolling, reducing the positive effect. The filler thickness also has an optimum range. Single-layer graphene (SLG) has the highest *intrinsic* thermal conductivity.[1,3] However, the thermal conductivity of SLG also suffers the most from the interaction with the matrix material.[3] At the opposite extreme, FLG with the thickness approaching milled graphite becomes a less efficient filler because it loses its mechanical flexibility. The latter results in a weaker coupling to the matrix, i.e., larger thermal contact resistance. Achieving a high loading of fillers required the use of commercial graphene and *h*-BN powders with limited control of the thicknesses and lateral dimensions. We intentionally did not perform extra processing steps required for filler optimization to achieve the highest thermal conductivity. For consistency and comparison, we wanted to keep the graphene and the *h*-BN fillers approximately the same sizes, thicknesses, and lateral dimensions. Two different fillers undergo different changes subjected to the same processing steps, e.g., additional centrifugation to change the size of fillers or functionalization. For this reason, the task of filler size optimization for attaining the maximum thermal conductivity enhancement is reserved for a future study.

Theoretical Analysis and Simulations. We now turn to finding the best theoretical model which can describe the thermal conductivity of the composites over a wide range of f. It is needed in order to elucidate the mechanism of heat conduction in the high loading composites above the thermal percolation. Such a model would also be useful for practical applications of composites with graphene or *h*-BN fillers. We have attempted to fit the experimental data with several of the most common models, including the Maxwell−Garnett,[68] Lewis−Nielsen,[50,51] Agari,[69] and others.[70] Previously, it was shown that the Maxwell−Garnett effective medium model (EMM), with the correction for the thermal boundary resistance (TBR) between the fillers and matrix, works well for graphene composites with the low loading $f \leq 10$ vol % [ref 11]. We found that the EMM approach as well as some other classical models, e.g., geometrical mean model, do not work well for the graphene or *h*-BN composites over the examined range of the filler loading (see Figures S5 and S6). We succeeded with the semi-empirical model of Lewis−Nielsen, which provided the best fitting to the experimental data over the entire range of the loading fractions (Figure 2a,b). This model explicitly takes into account the effect of the shape, packing of the particles, and, to some degree, their orientation with respect to the heat flux. In the framework of this model, the thermal conductivity is expressed as[51]

$$K/K_m = (1 + ABf)/(1 - B\psi f) \quad (1)$$

Here, the constant A is related to the generalized Einstein coefficient k_E as $A = k_E - 1$, and it depends on the shape of the fillers and their orientation with respect to the heat flow. The parameter $B = (K_f/K_m - 1)/(K_f/K_m + A)$ takes into account the relative thermal conductivity of the two phases: the fillers (K_f) and the base matrix (K_m), respectively. The parameter $\psi = 1 + ((1 - \phi_m)/\phi_m^2)f$ relates to the maximum packing fraction (ϕ_m) of the fillers. The values of A and ϕ_m are well tabulated for several different two-phase systems and can be found in refs 51 and 70. If the shape and packing of the fillers are known, the model predicts the thermal conductivity of the composites without other adjustable parameters.

The values of A and ϕ_m are not known for graphene, *h*-BN, or other quasi-2D flake-like fillers. Therefore, in this study, we used A and K_f as the fitting parameters to gain insight into the thermal transport in composites with the high loading of quasi-2D fillers. The maximum packing fraction ϕ_m was assumed to be 0.52, which corresponds to the three-dimensional randomly packed fillers inside the polymer matrix.[51] This is a reasonable assumption since, as the filler content increases beyond a certain value—the thermal percolation threshold—the fillers overlap with each other, creating randomly dispersed thermally conductive paths. Fitting our experimental data for the epoxy with graphene and *h*-BN fillers using the Lewis−Nielsen model gave us rather surprising results. First, the *apparent* thermal conductivity values of $K_f \sim 37$ W m^{-1} K^{-1} and $K_f \sim 16$ W m^{-1} K^{-1} have been extracted for graphene and *h*-BN fillers, respectively. These values are substantially lower than the intrinsic thermal conductivity of graphene and *h*-BN. Second, the values of A obtained from the fitting for two cases of epoxy with graphene and *h*-BN fillers are rather high: ∼61 and ∼31, respectively. It should be noted that parameter A depends on the shape and the aspect ratio of the filler, and as the aspect ratio increases, the value of A increases as well. For example, for randomly oriented rods with aspect ratios of 2, 4, 6, 10, and 15, the reported values of A are 1.58, 2.08, 2.8, 4.93, and 8.38,

DOI: 10.1021/acsami.8b16616
ACS Appl. Mater. Interfaces 2018, 10, 37555−37565

respectively.[51] The large A in our case demonstrates the creation of the rodlike thermal paths with very high aspect ratios. As $A \to \infty$, the Lewis–Nielsen model converges to the ordinary "rule of mixtures", which is $K = (1 - f)K_m + fK_f$, and as $A \to 0$, the model converges to the "inverse rule of mixtures", which is $1/K = (1 - f)/K_m + f/K_f$. The "rule of mixtures" and the "inverse rule of mixtures" provide the upper and lower bounds of the thermal conductivity of composites. Conceptually, the rule of mixtures considers the heat transfer along the two parallel paths of the fillers and the epoxy. For this reason, in our composites with the high loading of graphene and h-BN, described by the model with the large A and K_f/K_m ratio, most of the heat is being transferred by the percolated conductive fillers rather than the matrix.

An interesting question is the meaning of the low values of the *apparent* thermal conductivity of the fillers extracted from our experimental data by using the Lewis–Nielsen model. We argue that the low values are mostly defined by the apparent cross-plane thermal conductivity of the quasi-2D fillers rather than the detrimental effect of the matrix and defects, resulting in the decrease of the in-plane thermal conductivity of the fillers. The apparent cross-plane thermal conductivity can also include the thermal boundary resistance with another filler or matrix which can be altered via functionalization or other methods.[71−73] As follows from the discussion above, in our composites with $f \geq f_T$, the dominant, or significant fraction, of the heat propagates via the network of the thermally conductive fillers. In such a network of the overlapping quasi-2D graphene or h-BN fillers, the thermal transport is strongly affected by the out-of-plane thermal conductivity of FLG and h-BN fillers and TBR at the overlapping regions where the fillers are either directly attached to each other or separated by a thin epoxy layer. The heat has to propagate from one flake to another across their overlapping region (see the inset in Figure 3a). The cross-plane thermal conductivity of high-quality FLG can be *2 orders of magnitude* lower than the in-plane thermal conductivity of FLG fillers—very close to the average apparent values extracted by fitting the Lewis–Nielsen model to our experimental data. The two competing effects—the increase in heat conduction via creation of the thermally conductive filler pathways inside the polymer matrix and thermal resistance associated with the out-of-plane thermal transport at overlapping regions—explains a rather gradual change of the thermal conductivity of the composites at the thermal percolation limit as opposed to a very abrupt change in electrical conductivity at the electrical percolation limit. The thermal boundary resistance at the interface between two fillers or at the interface between the filler and epoxy matrix is also a factor, which prevents an abrupt enhancement of the thermal conductivity of the composite as the filler content exceeds the thermal percolation threshold. One can view the extracted thermal conductivity of the fillers as an average apparent quantity, which has contribution from the cross-plane thermal conductivity, implicitly includes TBR between the two overlapping flakes, and is affected by the filler exposure to the matrix material. The separation of the apparent cross-plane thermal conductivity on actual cross-plane thermal conductivity of the fillers and TBR does not add much to the present discussion.

To further confirm the conclusion based on the physical model fitting to the experimental data, we conducted a computational study, solving the steady-state heat diffusion equation for a composite region with two overlapping fillers.

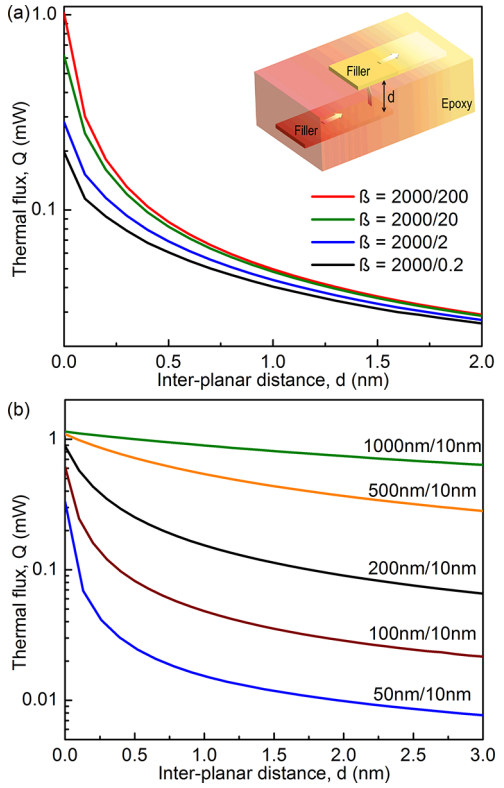

Figure 3. (a) Effect of filler's thermal conductivity anisotropy on heat flux across the overlapping fillers as a function of the interplanar distance between the fillers for 20% overlap at constant filler size aspect ratio AR = 100 nm/10 nm (length/thickness) and filler volume fraction of f = 28 vol %. The cross-plane thermal conductivity of the graphene fillers strongly affects the heat transfer in the case of the thermally percolated fillers. The inset shows schematically the heat propagation from one filler to the other (b). The effect of the aspect ratio on heat propagation in the percolated network for 20% overlap between the filler flakes. The results have been obtained for filler loading fraction of f = 28 vol % and thermal conductivity anisotropy of β = 2000/20 = 100. The increase of the filler lateral size, at fixed thickness, results in better heat conduction from one filler to another as compared to the case where the fillers are small.

The schematic of the system is shown in the inset of Figure 3a. We consider two identical graphene fillers with the lateral dimensions of 100 nm × 100 nm and the thickness of 10 nm, embedded in the epoxy. One 2D filler is on top of the other with the overlapping region of 20% of the filler's area. The heat flux is calculated as a function of the distance separating two fillers, starting from zero; i.e., the fillers are attached to each other, and going to the maximum distance of $d \approx 2$ nm. We consider several cases of the anisotropic thermal conductivity of the fillers defined by the ratio of the in-plane–to–cross-plane thermal conductivity $K_{\parallel-f}/K_{\perp-f} = \beta$. Since many of the fillers are FLG flakes, we use, for simplicity, the bulk graphite thermal conductivity for $K_{\parallel-f}$ = 2000 W m^{-1} K^{-1}. The value of $K_{\perp-f}$ varies to simulate the different degree of anisotropy. The high quality graphite has $K_{\perp-f}$ = 20 W m^{-1} K^{-1} at RT. One should understand that the $K_{\perp-f}$ value can implicitly include TBR at the interface between two fillers or filler-matrix material. It is modeled by taking $K_{\perp-f}$ = 0.2 W m^{-1} K^{-1}. The thermal conductivity of the epoxy matrix is taken as K_m = 0.2 W m^{-1} K^{-1}. The details of the simulations can be found in the Methods.

DOI: 10.1021/acsami.8b16616
ACS Appl. Mater. Interfaces 2018, 10, 37555−37565

Figure 3a shows the rate of heat flow, q, from the hot to the cold filler as a function of the interplanar distance, d, for different values of the cross-plane thermal conductivity of graphene fillers as shown in the legend. The in-plane thermal conductivity is fixed at 2000 W m^{-1} K^{-1}. When the fillers are touching (d = 0 nm), a lower cross-plane thermal conductivity results in a significant decrease in the heat flow from one filler to another. The decrease in the heat flow confirms the importance of the fillers' cross-plane thermal conductivity on heat transfer in the high loading composites, above the thermal percolation threshold. As the separation distance is increased to 2 nm, the effect of the cross-plane thermal conductivity becomes negligible. This situation is similar to that in dilute samples where there are no connections between the fillers. The observed trend explains why the thermal conductivity depends linearly on the loading at lower concentrations ($f < f_T$) and super-linearly on the loading at higher concentrations ($f > f_T$). At $f \leq f_T$, the heat is carried mostly via the epoxy matrix, in which the thermal conductivity is enhanced by separate islands of the fillers. However, at $f \geq f_T$, the heat is conducted mostly via the connected network of fillers with the apparent thermal conductivity limited by the cross-plane thermal conductivity, which is still an order of magnitude higher than that of the epoxy.

Figure 3b shows the thermal flux for a constant anisotropy of the thermal conductivity of β = 2000/20 = 100, as a function of the filler's aspect ratio (AR), defined as the ratio of the flake length to its thickness. We assumed the flakes have the same length and width. The increase of the filler lateral size, at fixed thickness, results in better heat conduction from one filler to another as compared to the case where the fillers are small. At very small aspect ratios, e.g., AR = 5, the heat transfer decreases abruptly as the separation distance d increases to ~1−2 nm. This indicates that the heat dissipates to the epoxy environment, which has very low thermal conductivity. The considered AR values are close to the experimental range; e.g., the flakes with micrometer lateral dimensions and 10 nm thickness have AR = 100. Practically, the upper bound for the filler size will be defined by the material processing technique and dimensions at which the fillers start to bend and roll over. One should also remember that, if the lateral dimension of the filler becomes smaller than the phonon MFP, its thermal conductivity starts to decrease due to onset of the ballistic phonon transport regime.[1−3]

While the percolation threshold loading fraction, f_T, is rather obvious in our case as the point where the linear dependence becomes super-linear (see Figures S5 and S6), there are no distinctive bends in the functional dependence (e.g., the derivative is smooth and continuous). In order to conclusively prove the change in the nature of thermal transport after reaching the percolation regime, we investigated the thermal diffusivity and thermal conductivity as the functions of temperature for the low-loading and high-loading composites. The studies were conducted in the temperature range from 295 to 385 K for the practical and fundamental science reasons. The examined range is the operational temperature of most of the electronic devices, and it represents a particular interest for developing TIMs and thermally conductive adhesives. This temperature range is also informative from the fundamental science point of view. In semiconductor and dielectric crystals, the most interesting range is between 20 and 80 K, where the thermal conductivity achieves its maximum. In completely disordered materials, e.g., amorphous carbon, the thermal conductivity monotonically increases well above room temperature.[3] In partially disordered materials, one can expect the maximum of the thermal conductivity slightly above RT. The behavior of the thermal conductivity of many composites in the low-temperature range is dominated by the specific heat dependence on temperature. Near RT and above, one has a chance to observe specifics of the phonon transport.

Thermal Diffusivity and Onset of Thermal Percolation. Figure 4a,b shows the thermal diffusivity, α, for composites with graphene and h-BN fillers. The thermal diffusivity of the samples has been measured using a laser flash technique (see Methods section and Figure S8). For the pristine epoxy and composites with the low filler content, the thermal diffusivity does not change with increasing temperature. The slope of the curves for the epoxy and epoxy with ~2 vol % of graphene and h-BN is in the order of 10^{-4} mm^2 s^{-1} K^{-1}. In the high loading composites, the thermal diffusivity decreases with increasing temperature. In samples with $f \geq 19$ vol %, the slope of the curves, which characterizes the rate of change of the diffusivity, is 10^{-2} mm^2 s^{-1} K^{-1}, 2 orders of magnitude larger than for the samples with $f \leq 3$ vol % of the filler loading. The change in the temperature dependence of the thermal diffusivity can be explained from the following considerations. Below the percolation limit, the heat is conducted mostly through the disordered matrix, with only a small fraction via the thermally conductive fillers. For this reason, the thermal diffusivity does not depend on temperature, or depends very weakly, as is typical for amorphous

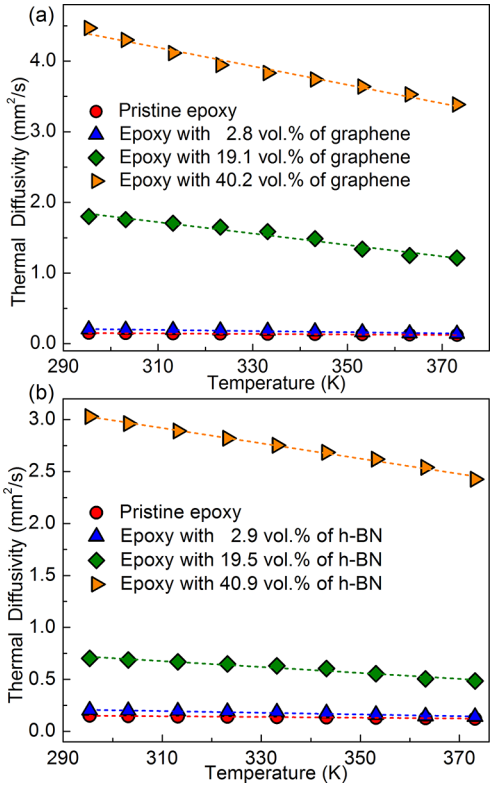

Figure 4. Thermal diffusivity of the epoxy composite with (a) graphene and (b) h-BN fillers as a function of temperature. For pristine epoxy and the low-filler-content composites, the thermal diffusivity does not change with increasing temperature. The thermal diffusivity reveals a decreasing trend with increasing temperature in the high-filler-content composites with the loading fraction $f \geq f_T$.

DOI: 10.1021/acsami.8b16616
ACS Appl. Mater. Interfaces 2018, 10, 37555−37565

materials in the examined temperature range. Above the percolation limit, heat mostly or partially travels via the percolation network, made from crystalline fillers such as graphene or *h*-BN. In this case, the temperature, T, dependence starts to evolve closer to the $1/T$ law, characteristic for crystalline solids above RT. In this sense, the change in $\alpha(T)$ functional dependence can be used as an additional criterion for distinguishing the onset of the percolation transport regime in the high loading composites.

The change in the nature of heat conduction above the thermal percolation limit becomes even more clear if one examines the temperature dependence of the thermal conductivity in the composites with the gradually changing filler content, from $f = 0$ to $f > f_T$ (see Figure 5). The thermal

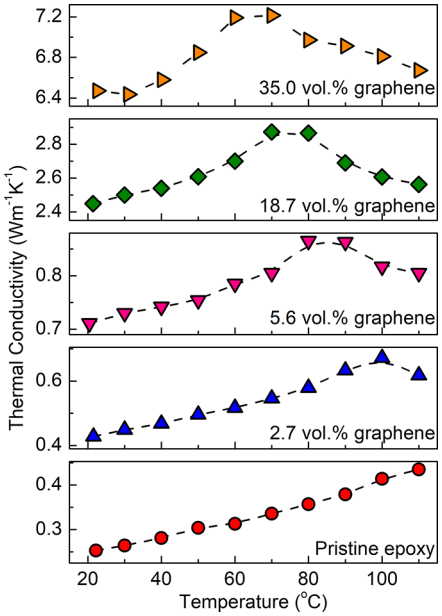

Figure 5. Thermal conductivity of the epoxy with graphene fillers as a function of temperature. The thermal conductivity of the pristine epoxy increases gradually with temperature as expected for amorphous or disordered materials. Addition of graphene results in the increase in the thermal conductivity and change in the thermal conductivity's dependence on temperature. Note an appearance of a pronounced maximum in the thermal conductivity and its shift to low temperatures as graphene filler content increases.

conductivity of the pristine epoxy increases slowly and monotonically in the temperature range from 295 to 385 K as expected for amorphous or disordered electrically insulating materials. As a small loading fraction of graphene (2.7 vol %) is added to the epoxy, the thermal conductivity shows a maximum at T_{max} = 373 K, and then starts to decrease. Addition of more graphene results in the increase of the thermal conductivity and the shift of T_{max} to lower temperatures owing to the gradual change of the structure of the composite from more amorphous to more crystalline due to the filler introduction. The maximum in thermal conductivity functional dependence on temperature, $K(T)$, is reminiscent of that in crystalline solids, although the maximum in our thermally percolated composites happens at substantially higher temperature.

CONCLUSIONS

In conclusion, we investigated the thermal conductivity and thermal diffusivity of epoxy composites with high loading fractions of graphene and *h*-BN fillers. It was found that both types of the composites revealed a *distinctive* thermal percolation threshold at a rather high loading fraction $f_T >$ 20 vol %. The changes in thermal transport at high loading fractions were confirmed by the temperature dependence of the thermal diffusivity. The graphene fillers outperformed boron nitride fillers in terms of thermal conductivity enhancement. It was also established that the thermal conductivity of both types of the composites can be best described by the Lewis–Nielsen model. The surprising finding is that, in the high loading composites with quasi-2D fillers, the apparent cross-plane thermal conductivity of the fillers can be the limiting factor for heat conduction. The obtained results are important for developing the next generation of the thermal interface materials.

METHODS

Sample Preparation. The composite samples were prepared by mixing commercially available few-layer graphene (Graphene Supermarket), *h*-BN (US Research Nanomaterials, Inc.), and epoxy (Allied High Tech Products, Inc.). Graphene and *h*-BN flakes were added to the epoxy resin at different mass ratios to prepare composites with varying filler contents. For samples containing a low filler loading fraction, the epoxy resin and the fillers were mixed using the high-shear speed mixer (Flacktek Inc.) at 800 rpm and then 2000 rpm each for 5 min. Then, the homogeneous mixture of epoxy and fillers were put inside a vacuum chamber for ∼10 min in order to extract the trapped air bubbles. The curing agent (Allied High Tech Products, Inc.) was then added in the prescribed mass ratio of 12:100 with respect to the epoxy resin. The solution was twice more mixed and vacuumed following the procedure outlined previously. Finally, the mixture was placed in an oven for ∼2 h at 70 °C to cure and solidify.

For the high-volume fraction samples, the graphene and *h*-BN fillers were added to the epoxy resin at several steps. In the first step, 1/3 of the total loading weight of the filler was added to half of the total weight of the required epoxy resin and was dispersed using a speed mixer at 2000 rpm for 5 min. Then, another 1/3 of the filler was mixed with the rest of the required epoxy resin. The solution was mixed one more time at 2000 rpm but for 10 min. The viscous mixture was then degassed in the vacuum chamber for 5 min. Afterward, the rest of the required graphene or *h*-BN was added with the curing agent to the mixture and stirred slowly using a homemade stirrer with the sharp needles. The needles helped to prevent filler agglomeration. At the next step, the composite was mixed at the high rotation speeds of 3500 and 2000 rpm for 15 s and 10 min, respectively. The homogeneous mixture was gently pressed and left in the oven at 70 °C for 2 h to cure. Using this procedure, several samples with a high filler loading of up to $f \approx 45$ vol % were successfully prepared.

Mass Density Measurements. To compare our thermal conductivity experimental results with available theoretical models, we converted the filler mass fraction ratio (φ) to the volume fraction (f) according to $f = \varphi\rho_m/(\varphi\rho_m + (1 - \varphi)\rho_f)$ equation. Here, ρ_m and ρ_f are the density of the epoxy and the filler, respectively. However, the density of the graphene and *h*-BN fillers can vary depending on the production method and possible impurities.[3,74] For this reason, we measured accurately the mass (m) and volume (V) of the disk-shaped samples and calculated the density of the composite samples according to $\rho = m/V$. Following an iterative procedure, we first assumed that the densities of the epoxy, graphene, and *h*-BN are 1.16, 2.26, and 2.16 g cm^{-3}. We converted the filler mass fraction of the samples to the filler volume fraction according to the aforementioned equation. We plotted the density of the composites versus the obtained volume fraction data and fitted the experimental data using a

DOI: 10.1021/acsami.8b16616
ACS Appl. Mater. Interfaces 2018, 10, 37555–37565

linear regression (see Figures S1 and S2). On the basis of the rule of mixtures for composites, $\rho = f(\rho_f - \rho_m) + \rho_m$, the y intercept of the fitted line and the slope will be equal to the density of the epoxy (ρ_m) and the difference between the filler and epoxy densities ($\rho_f - \rho_m$), respectively. Calculating the volume fraction based on the new values and following an iterative procedure discussed above, we extracted the exact values of the density for the fillers and the epoxy matrix. In our case, for epoxy with graphene fillers, the density of the graphene and epoxy was calculated as 1.16 g cm^{-3}and 2.16 g cm^{-3}, respectively. For the epoxy with h-BN fillers, the density of the h-BN and epoxy was calculated as 1.17 g cm^{-3} and 2.07 g cm^{-3}, respectively.

Thermal Conductivity Measurements. The thermal conductivity was measured using the transient plane source (TPS) "hot disk" technique. In the TPS method, an electrically insulated flat nickel sensor is placed between two pieces of the substrate. The sensor is working as the heater and thermometer simultaneously. A current pulse is passed through the sensor during the measurement to generate the heat wave. Thermal properties of the material are determined by recording temperature rise as a function of time. The time and the input power are chosen so that the heat flow is within the sample boundaries and the temperature rise of the sensor is not influenced by the outer boundaries of the sample. More details on the measurement procedures can be found in the Supporting Information and our prior reports on other material systems.[13,52,53,75−84]

Thermal Diffusivity Measurements. The measurements of the thermal diffusivity were performed by the transient "laser flash" (LFA) technique (NETZSCH LFA 447). The LFA technique uses a flash lamp, which heats the sample from one end by producing shot energy pulses. The temperature rise is determined at the back end with the infrared detector. The output of the temperature detector is amplified and adjusted for the initial ambient conditions. The recorded temperature rise curve is the change in the sample temperature resulting from the firing of the flash lamp. The magnitude of the temperature rise and the amount of the light energy are not required for the diffusivity measurement. Only the shape of the transient curve is used in the analysis. More details on the measurement procedures can be found in the Supporting Information and our prior reports on other material systems.[9,11,81,85]

Numerical Simulations. The heat conduction in the system consisting of the epoxy matrix and graphene fillers was calculated using the finite element method (FEM) as implemented in the COMSOL Multiphysics package. The FLG fillers were considered to be thermally anisotropic planes with the in-plane (out-of-plane) thermal conductivity $K_{\parallel}$ ($K_{\perp}$). The epoxy matrix was assumed to have uniform thermal conductivity K_m of 0.2 W m^{-1} K^{-1}. The interplanar distance, d, between the fillers was varied from zero to 10 nm. The heat transfer in the regions of the matrix (m) and graphene fillers (g) was described by their respective thermal conductivities $K_{m,g}$, as $\nabla \cdot (K_{m,g} \nabla T_{m,g}) = 0$. The fixed temperature boundary conditions were applied along the left and right faces of the simulation domain while all other faces were assumed to be adiabatic, $\partial T_m / \partial n_m = 0$, where n_m is the outward normal to the surface.

■ ASSOCIATED CONTENT

Supporting Information

The Supporting Information is available free of charge on the ACS Publications website at DOI: 10.1021/acsami.8b16616.

A detailed description of the composite preparation, mass density measurements, transient plane source "hot-disk" technique for the thermal conductivity measurements, "laser flash" experimental technique for the thermal diffusivity and conductivity measurements, as well as additional analysis of the thermal conductivity data (PDF)

■ AUTHOR INFORMATION

Corresponding Author

*E-mail: balandin@ece.ucr.edu. Web: http://balandingroup.ucr.edu/.

ORCID

Fariborz Kargar: 0000-0003-2192-2023

Author Contributions

‖These authors contributed equally to the work.

Author Contributions

A.A.B. and F.K. conceived the idea of the study. A.A.B. coordinated the project and contributed to the experimental and theoretical data analysis; F.K. conducted data analysis and assisted with the thermal measurements; Z.B. prepared the composites and performed electrical and thermal conductivity and diffusivity measurements with the help of R.S.; B.D. performed numerical modeling; J.S.L. conducted materials characterization; E.A. carried out Raman spectroscopy and related materials characterization. R.K.L. contributed to the theoretical and computational data analysis. A.A.B. led the manuscript preparation. All authors contributed to writing and editing of the manuscript.

Notes

The authors declare no competing financial interest.

■ ACKNOWLEDGMENTS

This work was supported, in part, by the National Science Foundation (NSF) through the Emerging Frontiers of Research Initiative (EFRI) 2-DARE award 1433395: Novel Switching Phenomena in Atomic MX_2 Heterostructures for Multifunctional Applications, and by the UC − National Laboratory Collaborative Research and Training Program "University of California Research Initiative" LFR-17-477237. A.A.B. also acknowledges NSF award 1404967: CDS&E Collaborative Research: Genetic Algorithm Driven Hybrid Computational − Experimental Engineering of Defects in Designer Materials.

■ REFERENCES

(1) Balandin, A. A.; Ghosh, S.; Bao, W.; Calizo, I.; Teweldebrhan, D.; Miao, F.; Lau, C. N. Superior Thermal Conductivity of Single-Layer Graphene. *Nano Lett.* **2008**, *8* (3), 902−907.

(2) Ghosh, S.; Calizo, I.; Teweldebrhan, D.; Pokatilov, E. P.; Nika, D. L.; Balandin, a. a.; Bao, W.; Miao, F.; Lau, C. N. Extremely High Thermal Conductivity of Graphene: Prospects for Thermal Management Applications in Nanoelectronic Circuits. *Appl. Phys. Lett.* **2008**, *92* (15), 151911.

(3) Balandin, A. A. Thermal Properties of Graphene and Nanostructured Carbon Materials. *Nat. Mater.* **2011**, *10* (8), 569−581.

(4) Ghosh, S.; Bao, W.; Nika, D. L.; Subrina, S.; Pokatilov, E. P.; Lau, C. N.; Balandin, A. a. Dimensional Crossover of Thermal Transport in Few-Layer Graphene. *Nat. Mater.* **2010**, *9* (7), 555−558.

(5) Seol, J. H.; Jo, I.; Moore, A. L.; Lindsay, L.; Aitken, Z. H.; Pettes, M. T.; Li, X.; Yao, Z.; Huang, R.; Broido, D.; Mingo, N.; Ruoff, R. S.; Shi, L. Two-Dimensional Phonon Transport in Supported Graphene. *Science* **2010**, *328* (5975), 213−216.

(6) Cai, W.; Moore, A. L.; Zhu, Y.; Li, X.; Chen, S.; Shi, L.; Ruoff, R. S. Thermal Transport in Suspended and Supported Monolayer Graphene Grown by Chemical Vapor Deposition. *Nano Lett.* **2010**, *10* (5), 1645−1651.

(7) Jauregui, L. A.; Yue, Y.; Sidorov, A. N.; Hu, J.; Yu, Q.; Lopez, G.; Jalilian, R.; Benjamin, D. K.; Delkd, D. A.; Wu, W.; Liu, Z.; Wang, X.; Jiang, Z.; Ruan, X.; Bao, J.; Pei, S. S.; Chen, Y. P. Thermal Transport

DOI: 10.1021/acsami.8b16616
ACS Appl. Mater. Interfaces 2018, 10, 37555−37565

in Graphene Nanostructures: Experiments and Simulations. *ECS Trans.* **2010**, *28*, 73−83.
(8) Yan, Z.; Liu, G.; Khan, J. M.; Balandin, A. A. Graphene Quilts for Thermal Management of High-Power GaN Transistors. *Nat. Commun.* **2012**, *3*, 827.
(9) Renteria, J.; Legedza, S.; Salgado, R.; Balandin, M. P. P.; Ramirez, S.; Saadah, M.; Kargar, F.; Balandin, A. A. Magnetically-Functionalized Self-Aligning Graphene Fillers for High-Efficiency Thermal Management Applications. *Mater. Des.* **2015**, *88*, 214−221.
(10) Shahil, K. M. F.; Balandin, A. a. Thermal Properties of Graphene and Multilayer Graphene: Applications in Thermal Interface Materials. *Solid State Commun.* **2012**, *152* (15), 1331−1340.
(11) Shahil, K. M. F.; Balandin, A. a. Graphene-Multilayer Graphene Nanocomposites as Highly Efficient Thermal Interface Materials. *Nano Lett.* **2012**, *12* (2), 861−867.
(12) Goli, P.; Ning, H.; Li, X.; Lu, C. Y.; Novoselov, K. S.; Balandin, A. A. Thermal Properties of Graphene−copper−graphene Heterogeneous Films. *Nano Lett.* **2014**, *14* (3), 1497−1503.
(13) Goli, P.; Legedza, S.; Dhar, A.; Salgado, R.; Renteria, J.; Balandin, A. a. Graphene-Enhanced Hybrid Phase Change Materials for Thermal Management of Li-Ion Batteries. *J. Power Sources* **2014**, *248*, 37−43.
(14) Saadah, M.; Hernandez, E.; Balandin, A. A. Thermal Management of Concentrated Multi-Junction Solar Cells with Graphene-Enhanced Thermal Interface Materials. *Appl. Sci.* **2017**, *7* (6), 589.
(15) Kargar, F.; Salgado, R.; Legedza, S.; Renteria, J.; Balandin, A. A. A Comparative Study of the Thermal Interface Materials with Graphene and Boron Nitride Fillers. *Proc. SPIE* **2014**, *9168*, 91680S−91680S−5.
(16) Fugallo, G.; Cepellotti, A.; Paulatto, L.; Lazzeri, M.; Marzari, N.; Mauri, F. Thermal Conductivity of Graphene and Graphite: Collective Excitations and Mean Free Paths. *Nano Lett.* **2014**, *14* (11), 6109−6114.
(17) Nika, D. L.; Ghosh, S.; Pokatilov, E. P.; Balandin, A. A. Lattice Thermal Conductivity of Graphene Flakes: Comparison with Bulk Graphite. *Appl. Phys. Lett.* **2009**, *94* (20), 203103.
(18) Fu, Y.-X.; He, Z.-X.; Mo, D.-C.; Lu, S.-S. Thermal Conductivity Enhancement of Epoxy Adhesive Using Graphene Sheets as Additives. *Int. J. Therm. Sci.* **2014**, *86*, 276−283.
(19) Shtein, M.; Nadiv, R.; Buzaglo, M.; Regev, O. Graphene-Based Hybrid Composites for Efficient Thermal Management of Electronic Devices. *ACS Appl. Mater. Interfaces* **2015**, *7* (42), 23725−23730.
(20) Aksamija, Z.; Knezevic, I. Lattice Thermal Conductivity of Graphene Nanoribbons: Anisotropy and Edge Roughness Scattering. *Appl. Phys. Lett.* **2011**, *98* (14), 141919.
(21) Chen, S.; Wu, Q.; Mishra, C.; Kang, J.; Zhang, H.; Cho, K.; Cai, W.; Balandin, A. A.; Ruoff, R. S. Thermal Conductivity of Isotopically Modified Graphene. *Nat. Mater.* **2012**, *11* (3), 203−207.
(22) Li, H.; Ying, H.; Chen, X.; Nika, D. L.; Cocemasov, A. I.; Cai, W.; Balandin, A. A.; Chen, S. Thermal Conductivity of Twisted Bilayer Graphene. *Nanoscale* **2014**, *6* (22), 13402−13408.
(23) Bae, M.-H.; Li, Z.; Aksamija, Z.; Martin, P. N.; Xiong, F.; Ong, Z.-Y.; Knezevic, I.; Pop, E. Ballistic to Diffusive Crossover of Heat Flow in Graphene Ribbons. *Nat. Commun.* **2013**, *4* (1), 1734.
(24) Xu, X.; Pereira, L. F. C.; Wang, Y.; Wu, J.; Zhang, K.; Zhao, X.; Bae, S.; Tinh Bui, C.; Xie, R.; Thong, J. T. L.; Hong, B. H.; Loh, K. P.; Donadio, D.; Li, B.; Özyilmaz, B. Length-Dependent Thermal Conductivity in Suspended Single-Layer Graphene. *Nat. Commun.* **2014**, *5* (1), 3689.
(25) Chen, L.; Xie, H.; Yu, W.; Wang, B.; Wu, Z. Thermal Transport Behaviors of Suspended Graphene Sheets with Different Sizes. *Int. J. Therm. Sci.* **2015**, *94*, 221−227.
(26) Bujard, P. Thermal Conductivity of Boron Nitride Filled Epoxy Resin: Temperature Dependence and Influence of Sample Preparation. In *InterSociety Conference on Thermal Phenomena in the Fabrication and Operation of Electronic Components(I-THERM '88)*, Los Angeles, CA, May 11−13, 1988; IEEE, 1988; pp 41−49..
(27) Shenogina, N.; Shenogin, S.; Xue, L.; Keblinski, P. On the Lack of Thermal Percolation in Carbon Nanotube Composites. *Appl. Phys. Lett.* **2005**, *87* (13), 133106.
(28) Bonnet, P.; Sireude, D.; Garnier, B.; Chauvet, O. Thermal Properties and Percolation in Carbon Nanotube-Polymer Composites. *Appl. Phys. Lett.* **2007**, *91* (20), 201910.
(29) Zheng, R.; Gao, J.; Wang, J.; Feng, S. P.; Ohtani, H.; Wang, J.; Chen, G. Thermal Percolation in Stable Graphite Suspensions. *Nano Lett.* **2012**, *12* (1), 188−192.
(30) Shtein, M.; Nadiv, R.; Buzaglo, M.; Kahil, K.; Regev, O. Thermally Conductive Graphene-Polymer Composites: Size, Percolation, and Synergy Effects. *Chem. Mater.* **2015**, *27* (6), 2100−2106.
(31) Gu, J.; Xie, C.; Li, H.; Dang, J.; Geng, W.; Zhang, Q. Thermal Percolation Behavior of Graphene Nanoplatelets/Polyphenylene Sulfide Thermal Conductivity Composites. *Polym. Compos.* **2014**, *35* (6), 1087−1092.
(32) Choi, S. U. S.; Zhang, Z. G.; Yu, W.; Lockwood, F. E.; Grulke, E. A. Anomalous Thermal Conductivity Enhancement in Nanotube Suspensions. *Appl. Phys. Lett.* **2001**, *79* (14), 2252−2254.
(33) Ding, Y.; Alias, H.; Wen, D.; Williams, R. A. Heat Transfer of Aqueous Suspensions of Carbon Nanotubes (CNT Nanofluids). *Int. J. Heat Mass Transfer* **2006**, *49* (1−2), 240−250.
(34) Prasher, R. Thermal Interface Materials: Historical Perspective, Status, and Future Directions. *Proc. IEEE* **2006**, *94* (8), 1571−1586.
(35) Stankovich, S.; Dikin, D. A.; Dommett, G. H. B.; Kohlhaas, K. M.; Zimney, E. J.; Stach, E. A.; Piner, R. D.; Nguyen, S. B. T.; Ruoff, R. S. Graphene-Based Composite Materials. *Nature* **2006**, *442* (7100), 282−286.
(36) Biercuk, M. J.; Llaguno, M. C.; Radosavljevic, M.; Hyun, J. K.; Johnson, A. T.; Fischer, J. E. Carbon Nanotube Composites for Thermal Management. *Appl. Phys. Lett.* **2002**, *80* (15), 2767−2769.
(37) Pang, H.; Chen, T.; Zhang, G.; Zeng, B.; Li, Z.-M. An Electrically Conducting Polymer/Graphene Composite with a Very Low Percolation Threshold. *Mater. Lett.* **2010**, *64* (20), 2226−2229.
(38) Zhang, H. B.; Zheng, W. G.; Yan, Q.; Yang, Y.; Wang, J. W.; Lu, Z. H.; Ji, G. Y.; Yu, Z. Z. Electrically Conductive Polyethylene Terephthalate/Graphene Nanocomposites Prepared by Melt Compounding. *Polymer* **2010**, *51* (5), 1191−1196.
(39) Martin, C. A.; Sandler, J. K. W.; Shaffer, M. S. P.; Schwarz, M. K.; Bauhofer, W.; Schulte, K.; Windle, A. H. Formation of Percolating Networks in Multi-Wall Carbon-Nanotube-Epoxy Composites. *Compos. Sci. Technol.* **2004**, *64* (15), 2309−2316.
(40) Awasthi, K.; Awasthi, S.; Srivastava, A.; Kamalakaran, R.; Talapatra, S.; Ajayan, P. M.; Srivastava, O. N. Synthesis and Characterization of Carbon Nanotube-Polyethylene Oxide Composites. *Nanotechnology* **2006**, *17* (21), 5417−5422.
(41) Potts, J. R.; Dreyer, D. R.; Bielawski, C. W.; Ruoff, R. S. Graphene-Based Polymer Nanocomposites. *Polymer* **2011**, *52* (1), 5−25.
(42) Li, A.; Zhang, C.; Zhang, Y.-F. Thermal Conductivity of Graphene-Polymer Composites: Mechanisms, Properties, and Applications. *Polymers* **2017**, *9* (12), 437.
(43) Bar-Cohen, A.; Matin, K.; Narumanchi, S. Nanothermal Interface Materials: Technology Review and Recent Results. *J. Electron. Packag.* **2015**, *137* (4), 040803−040817.
(44) Hansson, J.; Zandén, C.; Ye, L.; Liu, J. Review of Current Progress of Thermal Interface Materials for Electronics Thermal Management Applications. In *2016 IEEE 16th International Conference on Nanotechnology (IEEE-NANO)*, Sendai, Japan, 2016; IEEE, 2016; pp 371−374..
(45) Hernandez, Y.; Nicolosi, V.; Lotya, M.; Blighe, F. M.; Sun, Z.; De, S.; McGovern, I. T.; Holland, B.; Byrne, M.; Gun'Ko, Y. K.; Boland, J. J.; Niraj, P.; Duesberg, G.; Krishnamurthy, S.; Goodhue, R.; Hutchison, J.; Scardaci, V.; Ferrari, A. C.; Coleman, J. N. High-Yield Production of Graphene by Liquid-Phase Exfoliation of Graphite. *Nat. Nanotechnol.* **2008**, *3* (9), 563−568.
(46) Lotya, M.; Hernandez, Y.; King, P. J.; Smith, R. J.; Nicolosi, V.; Karlsson, L. S.; Blighe, F. M.; De, S.; Wang, Z.; McGovern, I. T.; Duesberg, G. S.; Coleman, J. N. Liquid Phase Production of

DOI: 10.1021/acsami.8b16616
ACS Appl. Mater. Interfaces 2018, 10, 37555−37565

Graphene by Exfoliation of Graphite in Surfactant/Water Solutions. *J. Am. Chem. Soc.* **2009**, *131* (10), 3611−3620.
(47) Allen, M. J.; Tung, V. C.; Kaner, R. B. Honeycomb Carbon: A Review of Graphene. *Chem. Rev.* **2010**, *110* (1), 132−145.
(48) Nethravathi, C.; Rajamathi, M. Chemically Modified Graphene Sheets Produced by the Solvothermal Reduction of Colloidal Dispersions of Graphite Oxide. *Carbon* **2008**, *46* (14), 1994−1998.
(49) Stankovich, S.; Dikin, D. A.; Piner, R. D.; Kohlhaas, K. A.; Kleinhammes, A.; Jia, Y.; Wu, Y.; Nguyen, S. B. T.; Ruoff, R. S. Synthesis of Graphene-Based Nanosheets via Chemical Reduction of Exfoliated Graphite Oxide. *Carbon* **2007**, *45* (7), 1558−1565.
(50) Nielsen, L. E. Thermal Conductivity of Particulate-Filled Polymers. *J. Appl. Polym. Sci.* **1973**, *17* (12), 3819−3820.
(51) Nielsen, L. E. The Thermal and Electrical Conductivity of Two-Phase Systems. *Ind. Eng. Chem. Fundam.* **1974**, *13* (1), 17−20.
(52) Gustafsson, S. E. Transient Plane Source Techniques for Thermal Conductivity and Thermal Diffusivity Measurements of Solid Materials. *Rev. Sci. Instrum.* **1991**, *62* (3), 797−804.
(53) Gustavsson, M.; Karawacki, E.; Gustafsson, S. E. Thermal Conductivity, Thermal Diffusivity, and Specific Heat of Thin Samples from Transient Measurements with Hot Disk Sensors. *Rev. Sci. Instrum.* **1994**, *65* (12), 3856−3859.
(54) Jo, I.; Pettes, M. T.; Kim, J.; Watanabe, K.; Taniguchi, T.; Yao, Z.; Shi, L. Thermal Conductivity and Phonon Transport in Suspended Few-Layer Hexagonal Boron Nitride. *Nano Lett.* **2013**, *13* (2), 550−554.
(55) Wang, C.; Guo, J.; Dong, L.; Aiyiti, A.; Xu, X.; Li, B. Superior Thermal Conductivity in Suspended Bilayer Hexagonal Boron Nitride. *Sci. Rep.* **2016**, *6* (1), 25334.
(56) Zhou, H.; Zhu, J.; Liu, Z.; Yan, Z.; Fan, X.; Lin, J.; Wang, G.; Yan, Q.; Yu, T.; Ajayan, P. M.; Tour, J. M. High Thermal Conductivity of Suspended Few-Layer Hexagonal Boron Nitride Sheets. *Nano Res.* **2014**, *7* (8), 1232−1240.
(57) Sichel, E. K.; Miller, R. E.; Abrahams, M. S.; Buiocchi, C. J. Heat Capacity and Thermal Conductivity of Hexagonal Pyrolytic Boron Nitride. *Phys. Rev. B* **1976**, *13* (10), 4607−4611.
(58) Sevik, C.; Kinaci, A.; Haskins, J. B.; Çağın, T. Influence of Disorder on Thermal Transport Properties of Boron Nitride Nanostructures. *Phys. Rev. B: Condens. Matter Mater. Phys.* **2012**, *86* (7), 075403.
(59) Sevik, C.; Kinaci, A.; Haskins, J. B.; Çağın, T. Characterization of Thermal Transport in Low-Dimensional Boron Nitride Nanostructures. *Phys. Rev. B: Condens. Matter Mater. Phys.* **2011**, *84* (8), 085409.
(60) Lindsay, L.; Broido, D. A. Theory of Thermal Transport in Multilayer Hexagonal Boron Nitride and Nanotubes. *Phys. Rev. B: Condens. Matter Mater. Phys.* **2012**, *85* (3), 035436.
(61) Cepellotti, A.; Fugallo, G.; Paulatto, L.; Lazzeri, M.; Mauri, F.; Marzari, N. Phonon Hydrodynamics in Two-Dimensional Materials. *Nat. Commun.* **2015**, *6* (1), 6400.
(62) Barrios-Vargas, J. E.; Mortazavi, B.; Cummings, A. W.; Martinez-Gordillo, R.; Pruneda, M.; Colombo, L.; Rabczuk, T.; Roche, S. Electrical and Thermal Transport in Coplanar Polycrystalline Graphene−hBN Heterostructures. *Nano Lett.* **2017**, *17* (3), 1660−1664.
(63) Illera, S.; Pruneda, M.; Colombo, L.; Ordejón, P. Thermal and Transport Properties of Pristine Single-Layer Hexagonal Boron Nitride: A First Principles Investigation. *Phys. Rev. Mater.* **2017**, *1* (4), 044006.
(64) Tian, W.; Yang, R. Phonon Transport and Thermal Conductivity Percolation in Random Nanoparticle Composites. *Comput. Model. Eng. Sci.* **2008**, *24* (2−3), 123−141.
(65) Guoqing Zhang; Yanping Xia; Hui Wang; Yu Tao; Guoliang Tao; Shantung Tu; Haiping Wu. A Percolation Model of Thermal Conductivity for Filled Polymer Composites. *J. Compos. Mater.* **2010**, *44* (8), 963−970.
(66) Kim, B. W.; Pfeifer, S.; Park, S. H.; Bandaru, P. R. The Experimental Determination of the Onset of Electrical and Thermal Conductivity Percolation Thresholds in Carbon Nanotube-Polymer Composites. *Mater. Res. Soc. Symp. Proc.* **2011**, *1312*, 281−286.
(67) Wattanakul, K.; Manuspiya, H.; Yanumet, N. Thermal Conductivity and Mechanical Properties of BN-Filled Epoxy Composite: Effects of Filler Content, Mixing Conditions, and BN Agglomerate Size. *J. Compos. Mater.* **2011**, *45* (19), 1967−1980.
(68) Garnett, J. C. M. Colours in Metal Glasses, in Metallic Films, and in Metallic Solutions. II. *Philos. Trans. R. Soc., A* **1906**, 237−288.
(69) Agari, Y.; Uno, T. Estimation on Thermal Conductivities of Filled Polymers. *J. Appl. Polym. Sci.* **1986**, *32* (7), 5705−5712.
(70) Pietrak, K.; Winiewski, T. S. A Review of Models for Effective Thermal Conductivity of Composite Materials. *J. Power Technol.* **2015**, *95* (1), 14−24.
(71) Walton, S. G.; Foley, B. M.; Hernández, S. C.; Boris, D. R.; Baraket, M.; Duda, J. C.; Robinson, J. T.; Hopkins, P. E. Plasma-Based Chemical Functionalization of Graphene to Control the Thermal Transport at Graphene-Metal Interfaces. *Surf. Coat. Technol.* **2017**, *314*, 148−154.
(72) Hopkins, P. E.; Baraket, M.; Barnat, E. V.; Beechem, T. E.; Kearney, S. P.; Duda, J. C.; Robinson, J. T.; Walton, S. G. Manipulating Thermal Conductance at Metal-Graphene Contacts via Chemical Functionalization. *Nano Lett.* **2012**, *12* (2), 590−595.
(73) Foley, B. M.; Hernández, S. C.; Duda, J. C.; Robinson, J. T.; Walton, S. G.; Hopkins, P. E. Modifying Surface Energy of Graphene via Plasma-Based Chemical Functionalization to Tune Thermal and Electrical Transport at Metal Interfaces. *Nano Lett.* **2015**, *15* (8), 4876−4882.
(74) Levinshtein, M. E.; Rumyantsev, S. L.; Shur, M. S., Eds. *Properties of Advanced Semiconductor Materials: GaN, AlN, InN, BN, SiC, SiGe*; John Wiley & Sons: New York, 2001.
(75) Parvizi, F.; Teweldebrhan, D.; Ghosh, S.; Calizo, I.; Balandin, A. A.; Zhu, H.; Abbaschian, R. Properties of Graphene Produced by the High Pressure-High Temperature Growth Process. *Micro Nano Lett.* **2008**, *3* (1), 29−34.
(76) Shamsa, M.; Ghosh, S.; Calizo, I.; Ralchenko, V.; Popovich, A.; Balandin, A. A. Thermal Conductivity of Nitrogenated Ultrananocrystalline Diamond Films on Silicon. *J. Appl. Phys.* **2008**, *103* (8), 083538.
(77) Ghosh, S.; Teweldebrhan, D.; Morales, J. R.; Garay, J. E.; Balandin, A. A. Thermal Properties of the Optically Transparent Pore-Free Nanostructured Yttria-Stabilized Zirconia. *J. Appl. Phys.* **2009**, *106* (11), 113507.
(78) Teweldebrhan, D.; Goyal, V.; Balandin, A. A. Exfoliation and Characterization of Bismuth Telluride Atomic Quintuples and Quasi-Two-Dimensional Crystals. *Nano Lett.* **2010**, *10* (4), 1209−1218.
(79) Goyal, V.; Sumant, A. V.; Teweldebrhan, D.; Balandin, A. A. Direct Low-Temperature Integration of Nanocrystalline Diamond with GaN Substrates for Improved Thermal Management of High-Power Electronics. *Adv. Funct. Mater.* **2012**, *22* (7), 1525−1530.
(80) Koo, B.; Goli, P.; Sumant, A. V.; dos Santos Claro, P. C.; Rajh, T.; Johnson, C. S.; Balandin, A. A.; Shevchenko, E. V. Toward Lithium Ion Batteries with Enhanced Thermal Conductivity. *ACS Nano* **2014**, *8* (7), 7202−7207.
(81) Ramirez, S.; Chan, K.; Hernandez, R.; Recinos, E.; Hernandez, E.; Salgado, R.; Khitun, A. G.; Garay, J. E.; Balandin, A. A. Thermal and Magnetic Properties of Nanostructured Densified Ferrimagnetic Composites with Graphene - Graphite Fillers. *Mater. Des.* **2017**, *118*, 75−80.
(82) Volodchenkov, A. D.; Ramirez, S.; Samnakay, R.; Salgado, R.; Kodera, Y.; Balandin, A. A.; Garay, J. E. Magnetic and Thermal Transport Properties of SrFe12O19 Permanent Magnets with Anisotropic Grain Structure. *Mater. Des.* **2017**, *125*, 62−68.
(83) Chung, E.; Paul, D.; Balakrishnan, G.; Lees, M.; Ivanov, A.; Yethiraj, M. Role of Electronic Correlations on the Phonon Modes of MnO and NiO. *Phys. Rev. B: Condens. Matter Mater. Phys.* **2003**, *68* (14), 140406.
(84) Lee, E.; Salgado, R. A.; Lee, B.; Sumant, A. V.; Rajh, T.; Johnson, C.; Balandin, A. A.; Shevchenko, E. V. Design of Lithium Cobalt Oxide Electrodes with High Thermal Conductivity and

DOI: 10.1021/acsami.8b16616
ACS Appl. Mater. Interfaces 2018, 10, 37555−37565

Electrochemical Performance Using Carbon Nanotubes and Diamond Particles. *Carbon* **2018**, *129*, 702−710.
(85) Kargar, F.; Ramirez, S.; Debnath, B.; Malekpour, H.; Lake, R. R. K.; Balandin, A. A. Acoustic Phonon Spectrum and Thermal Transport in Nanoporous Alumina Arrays. *Appl. Phys. Lett.* **2015**, *107* (17), 171904.

DOI: 10.1021/acsami.8b16616
ACS Appl. Mater. Interfaces 2018, 10, 37555−37565